Electronic Supplementary Material (ESI) for RSC Advances.

Supporting Information

Atomically Dispersed Cu on $Ce_{1-x}RE_xO_{2-\delta}$ nanocubes (RE = La and Pr) for Water Gas Shift: Influence of OSC on Catalysis

Muhammad Ridwan,[a,c] Rizcky Tamarany,[a] Jonghee Han, [a,b] Suk Woo Nam,[a,b] Hyung Chul Ham,[a,c] Jin Young Kim,[a] Sun Hee Choi,[a] and Seong Cheol Jang,[a] Chang Won Yoon[a,c,*]

[a]Fuel Cell Research Center, Korea Institute of Science and Technology, Seoul 02792, Republic of Korea

[b]Green School, Korea University, Seoul 02841, Republic of Korea

[c]Department of Clean Energy and Chemical Engineering, Korea University of Science and Technology, Daejeon 34113, Republic of Korea

Experimental

Materials and characterization

Cerium nitrate hexahydrate ($Ce(NO_3)_3 \cdot 6H_2O$, Kanto Chemical Co., Inc.), Lanthanum nitrate hexahydrate ($La(NO_3)_3 \cdot 6H_2O$, Sigma-Aldrich) Praseodymium nitrate hexahydrate ($Pr(NO_3)_3 \cdot 6H_2O$, Alfa Aesar.) sodium hydroxide (NaOH, Junsei Chemical Co., Ltd.), anhydrous ethyl alcohol (Samchun Pure Chemical Co., Ltd.), copper methoxide ($Cu(OCH_3)_2$, Sigma-Aldrich), tetrahydrofuran (THF, Sigma-Aldrich), and tetrahydofuran-d^8 (Cambridge Isotope Laboratories Inc.) were purchased and employed as received without further purification.

XRD analyses were conducted using a Rigaku MiniFlex II X-ray diffractometer. Morphological studies with determination of particle size and distribution were conducted using high resolution transmission electron microscope (HR-TEM) using FEI Tecnai F20 at 200 kV. Surface elemental analyses (Cu loading) with morphological studies were carried out using scanning electron microscopy (SEM, Hitachi S-4200) in conjunction with energy dispersive X-ray analysis (EDS). The surface area of a catalyst was measured using a BET apparatus (ASAP 2000 Micromeritics). XPS was performed using PHI 5000 VersaProbe (Ulvac-PHI). Raman analysis was conducted with Renishaw (InVia Raman Microscope). To monitor the formation of byproducts generated during surface reactions between copper methoxide and surface hydroxyl group located at ceria surface, ^{1}H NMR spectroscopy (400 MHz FT NMR, Bruker) was employed. To measure the amounts of methanol produced during the surface reaction, acetone was employed as an internal standard for the NMR experiments.

Synthetic procedure for CeO_2 and RE-doped CeO_2 supports

Cubic CeO_2 nanocrystals were prepared by a modified procedure based on a previous report.[1] In a typical synthesis, $Ce(NO_3)_3 \cdot 6H_2O$ (14.0 g, 32.2 mmol) was dissolved in distilled water (100 mL) followed

by adding aqueous NaOH solution (final NaOH concentration, 8 M) upon stirring rapidly. The resulting slurry was then continuously stirred for overnight, which was then transferred into a Teflon lined autoclave reactor with an inner volume of 350 mL. The volume of the slurry solution filled in the reactor is about 86% of the volume of autoclave. The autoclave reactor was transferred into a furnace and heated up to 180 °C for 20 h. The reactor was then allowed to cool down to room temperature. The formed precipitates were separated by centrifugation with consecutive filtration, followed by washing several times with distilled water until the pH of the washed solution reached to be neutral. The obtained powders were dried in vacuum at room temperature for 12 h. RE-doped CeO_2 nanocubes (RE = La and Pr) were prepared with the same method as above.

To prepare irregular CeO_2 particles, $Ce(NO_3)_3.6H_2O$ (26 g, 0.059 mol), were dissolved in distilled water (75 mL) and an aqueous ammonia solution (225 mL, 0.8 M) was added to the CeO_2-H_2O mixture rapidly. The colloidal CeO_2 solution was then heated in Teflon lined autoclave at 100 °C for 24 h. The resulting yellow precipitates were filtered and dried under vacuum overnight.

Introducing copper into CeO_2: A molecular precursor approach

A solution containing copper methoxide ($Cu(OCH_3)_2$, 29 mg) as a Cu precursor and THF (100 mL) was stirred and agitated using a ultrasonicator for 30 min. The as-prepared CeO_2 particles (2 g) were added into the suspension, and the resulting mixture was stirred at 24 °C for 1 h. The suspension was then heated at 70 °C for 24 h, which enabled that the copper ions were completely anchored at the surface of the CeO_2 by a surface reaction (*vide infra*). The solids were separated using a centrifuge with consecutive filtration following the reaction, and further purified by washing with ethanol. The obtained catalysts were dried at 80 °C for 12 h, followed by calcination at 400 °C for 10 h with a ramping rate of 4 °C/min.

To compare catalytic activities of the Cu catalysts prepared using the molecular precursor approach with those produced by a conventional impregnation method, we further synthesized Cu/CeO_2 catalysts using $Cu(NO_3)_2$ by reduction using $NaBH_4$. A desired quantity of copper nitrate was dissolved in distilled water (100 mL). The calcined CeO_2 powders (2.0 g) were added to the aqueous solution and the suspension was stirred for 1 h. The $NaBH_4$ reductant with a $NaBH_4$:Cu molar ratio of 10:1 was added to this suspension with continuous stirring for 12 h. The formed precipitates were separated by filtration with consecutive washing. The obtained powders were dried in an oven preheated at 80 °C for overnight, followed by calcination at 400 °C for 10 h.

Thermogravimetric analysis for OSC calculation

A catalyst was initially heated from room temperature to 400 °C under air flow with a heating rate of 10 °C/min. At 400 °C, air flow with O_2 was stopped. N_2 gas was then supplied for 10 min to remove the filled oxygen from the catalyst, which resulted in weight loss. The repetition of the processes gave the quantities of oxygen vacancies in the catalyst. The amounts of oxygen vacancies were calculated using the following equation:

$$\text{The quantities of oxygen vacancy} = \frac{\left(g_{decreased\ weight} / g_{cat}\right)}{MW_{O_2}}$$

Where MW is the molecular weight of the oxygen.

Monitoring CH_3OH formation using ^1H NMR

To monitor the formation of methanol upon reaction between CeO_2 and copper methoxide the ^1H NMR analysis was used. CeO_2 powder (0.20 g) was dispersed into d^8-THF solvent then copper methoxide (2.9 mg) was added. The suspension was vigorously stirred and heated at 70°C for 24 h, followed by cooling down to room temperature. Acetone (40 µmol) was then added to the suspension

as an internal standard. The suspension was filtered, and the filtrate was loaded into a NMR tube for NMR analysis.

Catalytic water gas shift (WGS) reactions

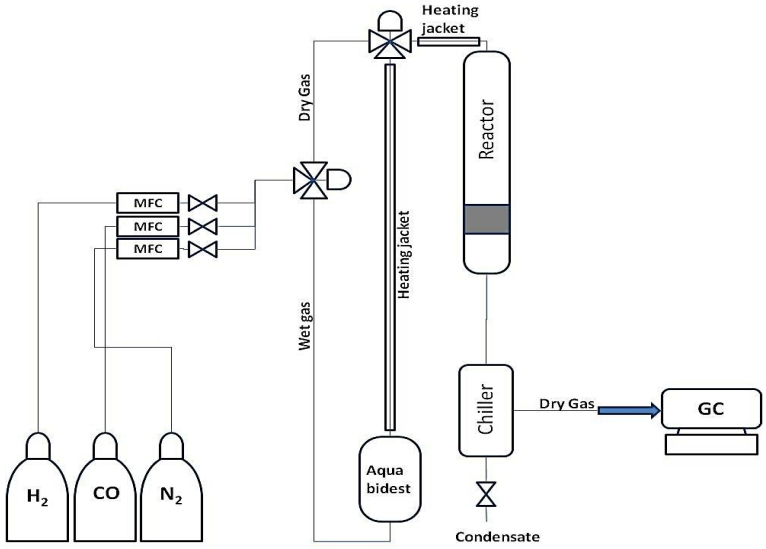

Figure SS1. A fixed bed reactor for water gas shift reaction.

The activities of the as-synthesized Cu based catalysts on water gas shift reactions were determined in a fixed-bed reactor with an inner diameter of 7.8 mm at ambient pressure (Figure SS1). In a typical experiment, the reactor containing a prepared catalyst (0.4 g) was heated to 350 ^{o}C in an electric furnace equipped with a K-type thermocouple. The temperature of the catalyst bed was monitored by a temperature controller (Hanyong Nux. co. Ltd). Prior to a desired reaction, a catalyst was reduced by 10% H_2 in N_2 at 350 °C for 3 h with a flow rate of 100 mL/min. The reactor was then flushed with N_2 for 60 min to decrease its temperature to 150 °C. The desired water gas shift reaction was carried out at temperature of 150 °C until 350 °C by supplying gases (CO, Steam, and N_2) at a GHSV of

25,500 h^{-1}, with the concentration of CO gas being fixed at 2.24 % mol, and steam with 13.44 % mol (CO: H_2O mol ratio is 1:6). N_2 was used as a tie component. Volumetric flows of hydrogen, nitrogen and carbon monoxide were controlled by digital mass flow controllers (MKP series, TSC-110 model). Compositions of the effluent gases were determined by an online gas chromatograph (Agilent 7890A) equipped with PorapakQ and Molecular sieve capillary columns as well as a thermal conductivity detector (TCD).

The turnover frequencies (TOFs) of the catalysts were calculated using the following equation.

$$TOF\ (h^{-1}) = \frac{X \times AW_M \times F}{W \times M}$$

Where X is the CO conversion (%)/100, AW_M is the atomic weight of Cu metal (g_{cu}/mol), F is the CO flow rate (mol/h), W is the mass of catalyst (g_{cat}), and M is the metal content (g_{Cu}/g_{cat}).

Computational Methods

DFT+U plane-wave calculations were performed using the Vienna ab initio simulation package (VASP).[2] The projector-augmented wave method (PAW) was used to describe the interaction between the ionic core and the valence electrons.[3] The exchange–correlation function was treated with the generalized gradient approximation (GGA) with the spin-polarized functional of Perdew-Burke-Ernzerhof (PBE).[4] A 400 eV cut-off energy was used. The Brillouin zone was sampled with the (4x4x4), (2x2x1), and (2x2x1) Monkhorst–Pack[5] mesh k-points for bulk, (2x2) CeO_2(111) slab, and (2x2) CeO_2(100) slab models, respectively. To avoid interactions between slabs, all slabs were separated by a vacuum space of 20 Å. In order to treat the highly localized Ce and Pr 4f-orbital, a Hubbard-U term with U_{eff} = 5 eV and U_{eff} = 4.5 eV were applied, respectively. For the La-doped CeO_2 system, we applied U_{eff} = 7 eV for O 2p states to

describe the generated-oxygen hole when La was doped into CeO_2.[6] The convergence criteria for the electronic structure and the geometry were 10^{-4} eV and 0.01 eV/Å, respectively.

The CeO_2(111) and (100) surfaces were contains with 48 Ce ; 96 O and 32 Ce ; 64 O, respectively. The (111) surface is representation of surface from CeO_2 irregular nanoparticles while (100) surface is a representation of surface from CeO_2 cubic nanocrystals. Figure S8 shows CeO_2(111) and (100) surfaces as periodically repeated slabs consisting of nine (three Ce-layers; six O-layers) and nine (four Ce-layers; five O-layers) atomic layers, respectively. The bottom six atomic layers of the CeO_2(111) and (100) surfaces, were fixed, while the remaining layers were fully relaxed. The La/Pr-doped CeO_2 was modeled by substitute La/Pr doping atom with Ce atoms in CeO_2(100) slab. In our model, La/Pr was located at the surface, since La and Pr tends to segregate onto CeO_2 surface.[7, 8]

The formation energy of O-vacancy were calculated using,

$$E_f^{Vo} = E_{CeO_2}^{Vo} + \frac{1}{2}E_{O_2}^{ref} - E_{CeO_2}$$

where, $E_{CeO_2}^{Vo}$ is total energy of CeO_2 surface with O-vacancy, E_{CeO_2} is total energy of CeO_2 surface without O-vacancy, and $\frac{1}{2}E_{O_2}^{ref}$ is reference energy of oxygen. In the calculation for O-vacancy formation energy at La-doped CeO_2(100), we calculated O_2 energy with U_{eff} = 7 eV.

Table and figures

Table S1. Integrated areas of individual peaks of XPS graph

Samples	Integrated Area of Peak				$[Ce^{3+}] / [Ce^{3+} + Ce^{4+}]$
	v	v′	v″	v‴	
1	8033	3719	6245	7334	15
2	4197	7406	7138	8329	27
3	1682	3733	4264	4015	27
4	836	2237	2783	2538	27

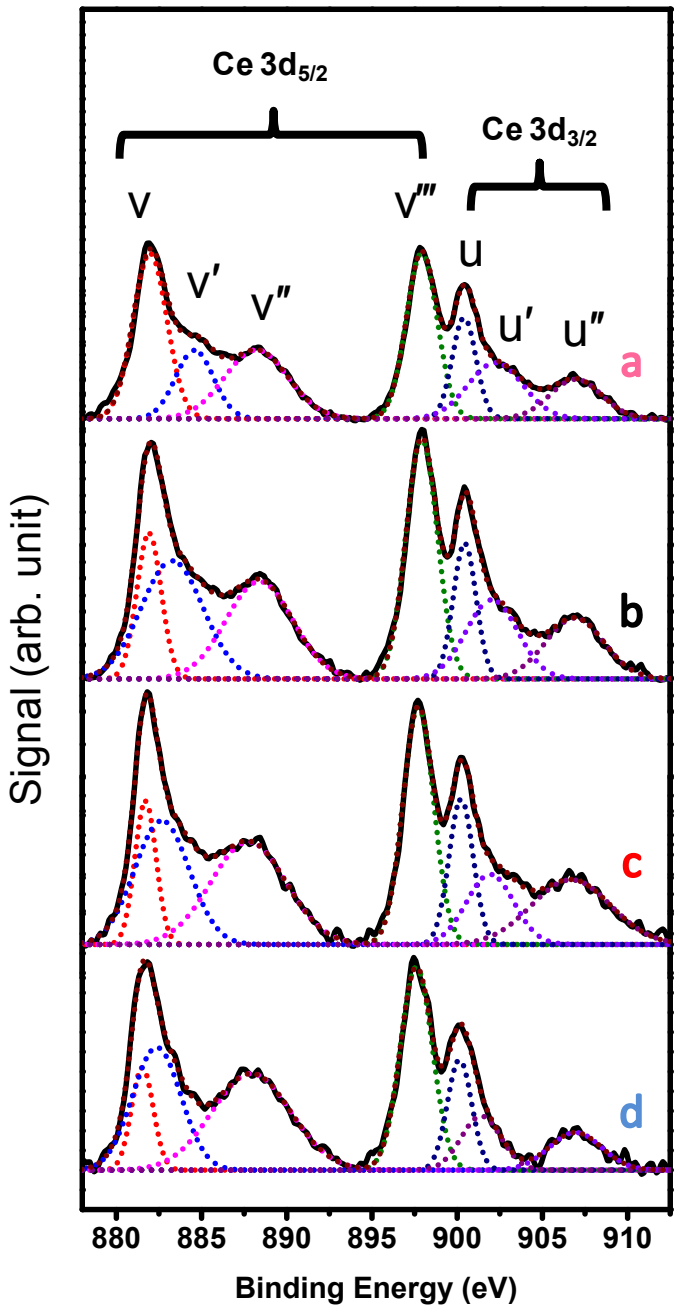

Figure S1. XPS spectra (Ce 3d) of the prepared CeO_2 materials: (a) CeO_2 irregular NPs (**1**), (b) CeO_2 nanocubes (**2**), (c) $Ce_{0.88}La_{0.12}O_{2-\delta}$ nanocubes (**3**), and (d) $Ce_{0.88}Pr_{0.12}O_{2-\delta}$ nanocubes (**4**).

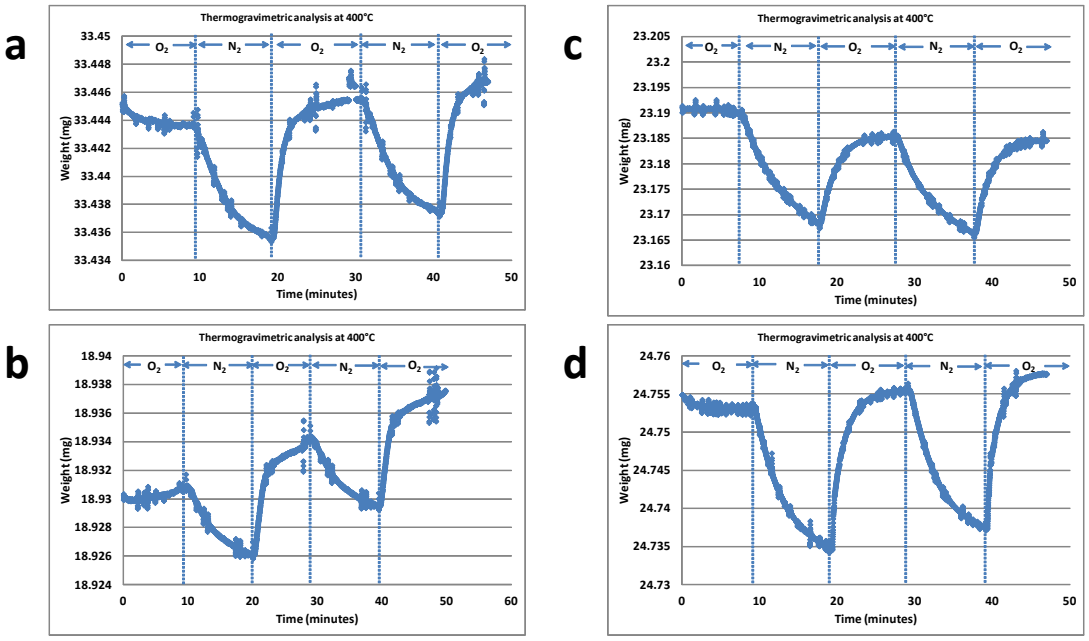

Figure S2. TGA profiles: (a) CeO_2 irregular NPs (**1**), (b) CeO_2 nanocubes (**2**), (c) $Ce_{0.88}La_{0.12}O_{2-\delta}$ nanocubes (**3**), and (d) $Ce_{0.88}Pr_{0.12}O_{2-\delta}$ nanocubes (**4**).

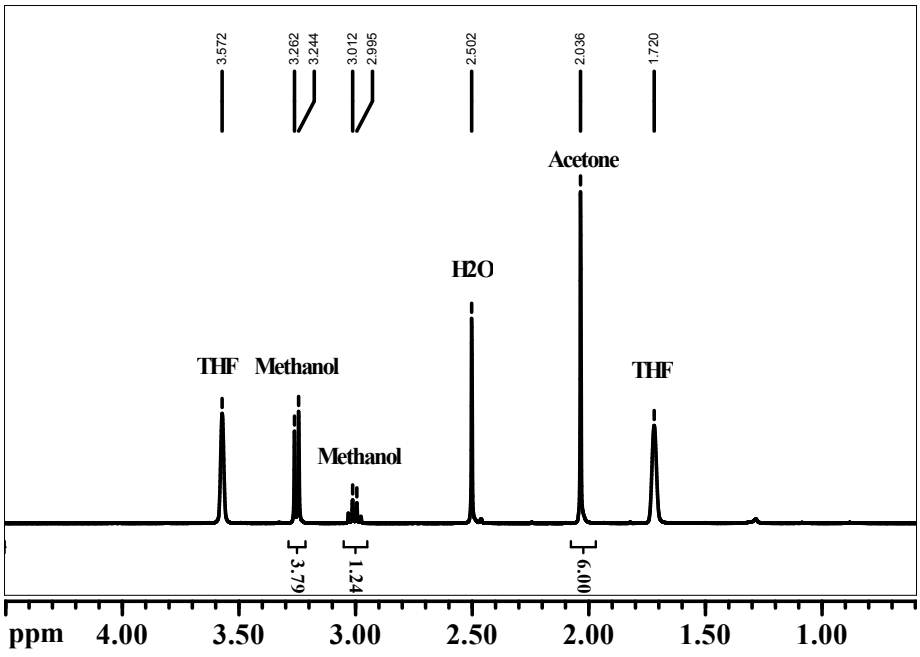

Figure S3. NMR spectra following the reaction of **2** and $Cu(OCH_3)_2$.

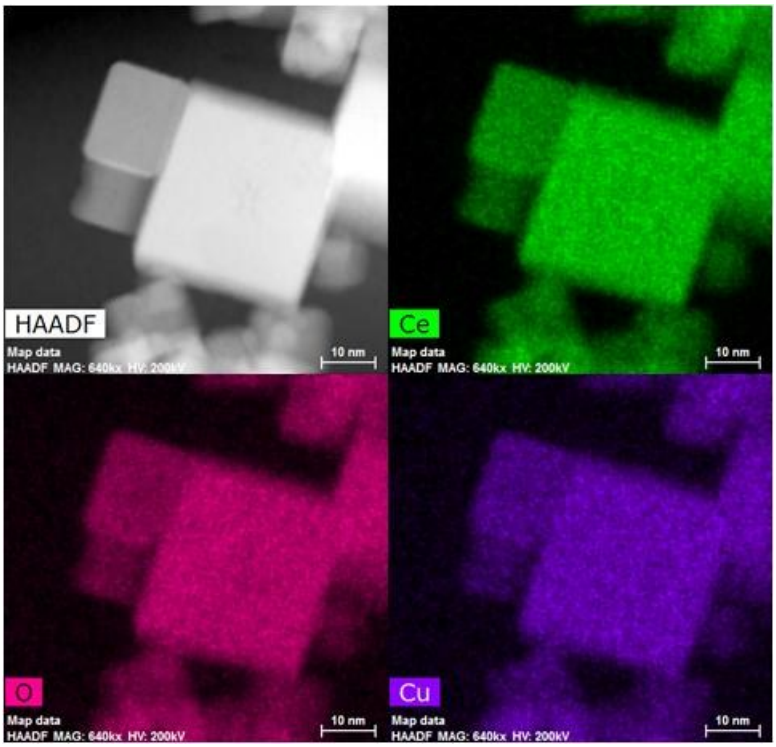

Figure S4. STEM-EDS mapping of **Cu-2** catalyst.

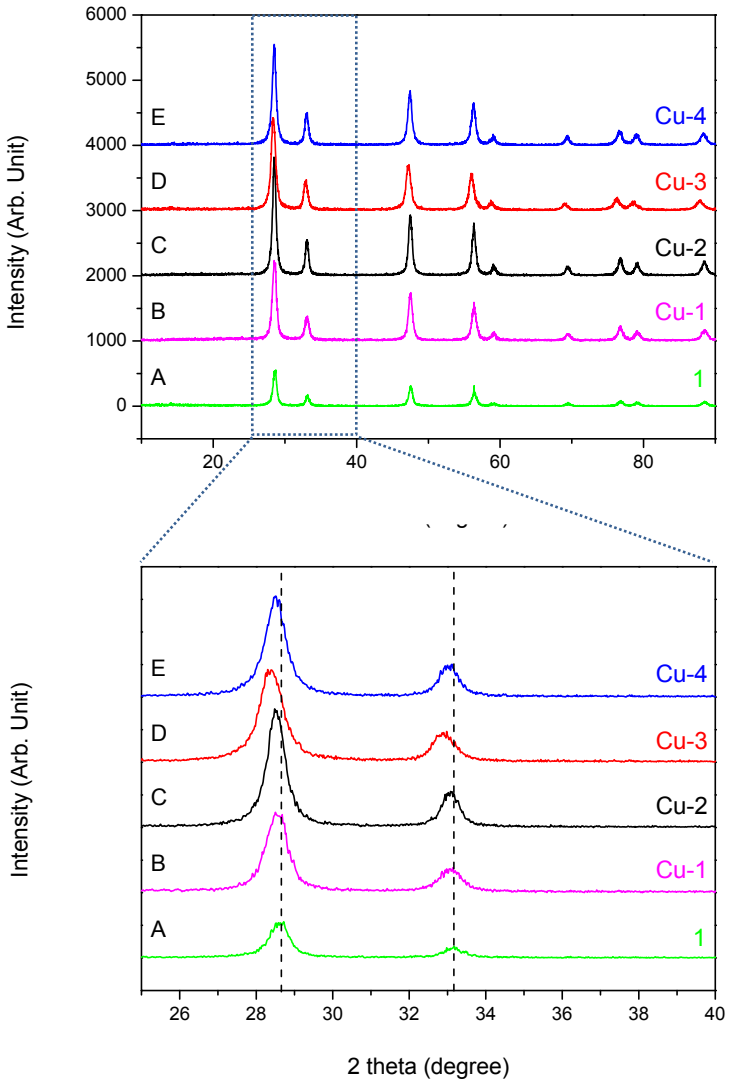

Figure S5. XRD spectra: (A) **1**, (B) **Cu-1**, (C) **Cu-2**, (D) **Cu-3**, and (E) **Cu-4**.

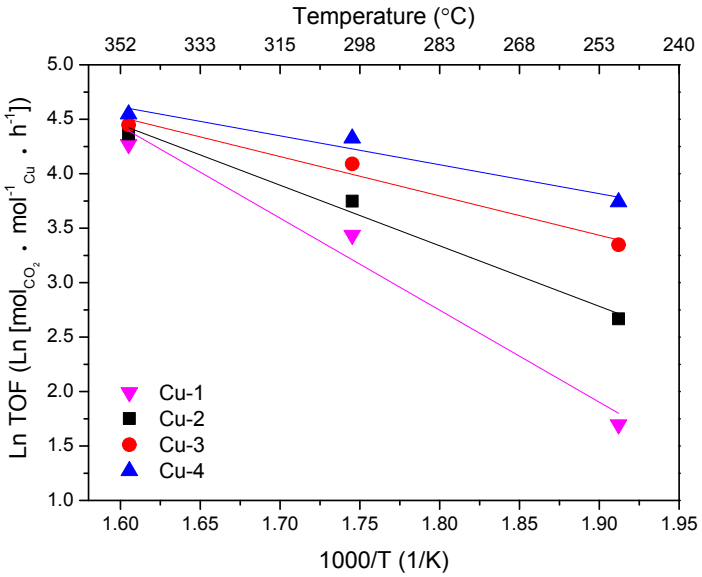

Figure S6. Arrhenius plot of TOF for the WGS reaction on Cu-1 (▼, pink), Cu-2 (■, black), Cu-3 (●, red), and (4) Cu-4 (▲, blue).

Table S2. TOF and activation energy data of WGS reaction on different samples

Sample	TOF (h^{-1})			E_a (kJ/mol)
	350°C	300°C	250°C	
Cu-1	71	31	5	70
Cu-2	79	42	14	46
Cu-3	85	60	28	30
Cu-4	94	76	42	22

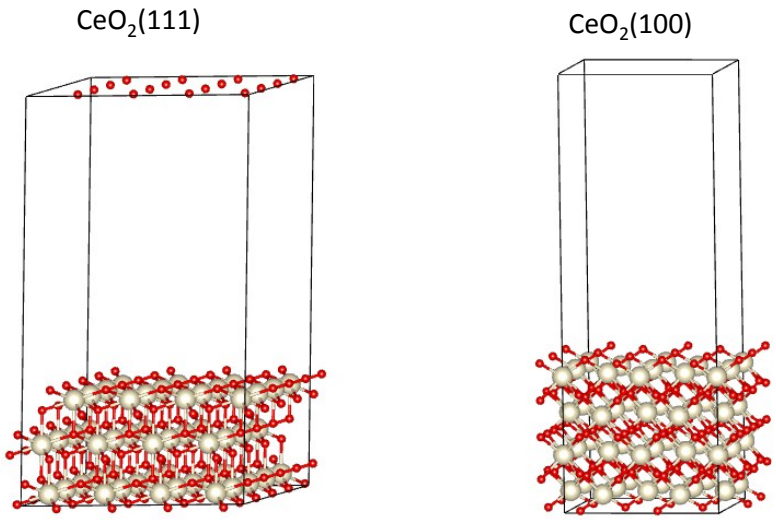

Figure S7. Periodic slab model for CeO_2(111) and CeO_2(100) surfaces. Red and white spheres represent oxygen and Ce atoms, respectively.

Table S3. Oxygen vacancy formation energies of model surfaces for **1** - **4**.

Surfaces	E_f^{Vo} (eV)	
	Our work (PBE+U^{Ce}_{eff} = 5 eV)	References
$Ce_{48}O_{96}$ (111)	2.27	2.34 (PBE+U^{Ce}_{eff} = 4.5 eV)[9] 2.60 (PW91+U^{Ce}_{eff} = 5 eV)[10]
$Ce_{32}O_{64}$ (100)	1.63	2.27 (PW91+U^{Ce}_{eff} = 5 eV)[10] 2.60 (HSE06)[11]
$Ce_{31}La_1O_{64}$ (100)	0.83	-
$Ce_{31}Pr_1O_{64}$ (100)	0.62	-

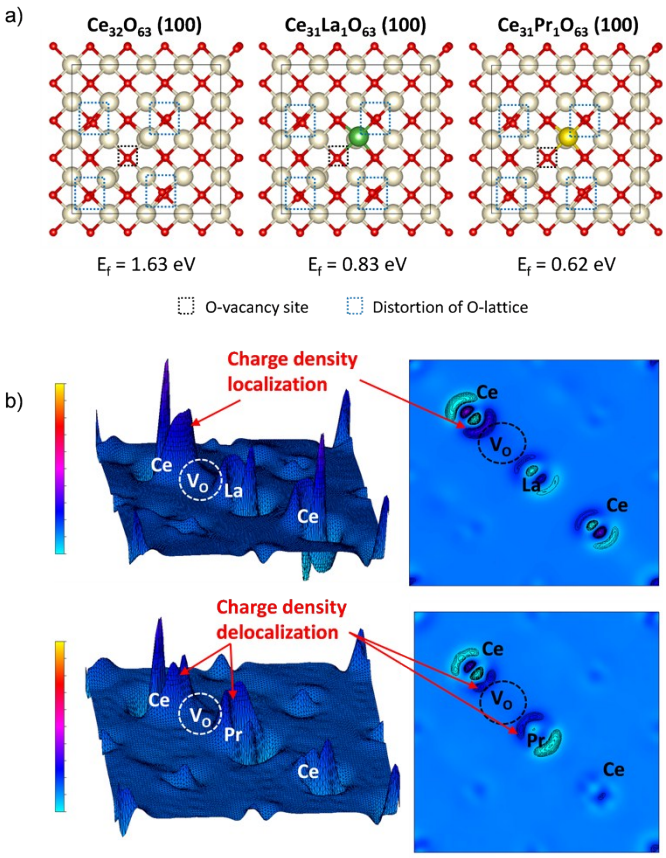

Figure S8. (a) Top view of $Ce_{32}O_{64}$(100) based surfaces with one oxygen vacancy with no dopant (left), La-doped (middle), and Pr-doped (right). Red, white, green, and yellow spheres represent oxygen, Ce, La, and Pr atoms, respectively. (b) 3D and 2D charge density difference for $Ce_{31}La_1O_{63}$(100) (upper) and $Ce_{31}Pr_1O_{63}$(100) (lower).

To further gain insight for the effect of both shape and La and Pr doping on OSC, DFT studies were conducted using four model catalyst surfaces, $Ce_{48}O_{96}(111)$, $Ce_{32}O_{64}(100)$, $Ce_{31}La_1O_{64}(100)$, and $Ce_{31}Pr_1O_{64}(100)$. In good agreement with the experimental results, the calculated oxygen vacancy formation energies show a decreasing tendency (Figure S8a and Table S3): $Ce_{48}O_{96}(111)$ (2.27 eV) > $Ce_{32}O_{64}(100)$ (1.63 eV) > $Ce_{31}La_1O_{64}(100)$ (0.83 eV) > $Ce_{31}Pr_1O_{64}(100)$ (0.62 eV). We further observed oxygen atom displacements upon formation of oxygen vacancies, leading to CeO_2 lattice distortions (Figure 5a, blue dotted square): for $Ce_{32}O_{63}(100)$, 0.010 Å; for $Ce_{31}La_1O_{63}(100)$, 0.014 Å; and for $Ce_{31}Pr_1O_{63}(100)$, 0.015 Å. Ahn et al. recently reported that the lattice distortions of CeO_2 enhanced the capability for oxygen vacancy migration through generated free space.[12]

The type of a dopant could also be a major controlling factor for oxygen vacancy formation of CeO_2 by involving charge distribution in a distinct manner. In this context, we further calculated differences in charge density between stoichiometric CeREO ($Ce_{31}RE_1O_{64}(100)$) and defective CeREO ($Ce_{31}RE_1O_{63}(100)$) ($\Delta\rho(r) = \rho_{stoichiometric}(r) - \rho_{O\text{-}vac}(r)$). For $Ce_{31}La_1O_{63}(100)$, it was revealed that the charges generated upon oxygen removal were localized mainly at Ce (Figure 5b, upper, see red arrow).. On the other hand, the charges produced following oxygen vacancy formation at $Ce_{31}Pr_1O_{63}(100)$ were delocalized at both Ce and Pr (Figure 5b, lower, see red arrow). This charge delocalization likely comes from the reducibility of Pr and may further contribute to stabilize the generated oxygen vacancy in the Pr-doped CeO_2.

References

1. Y. Zhiqiang, Z. Kebin, L. Xiangwen, T. Qun, L. Deyi and Y. Sen, *Nanotechnology*, 2007, **18**, 185606.
2. G. Kresse and J. Furthmüller, *Physical Review B*, 1996, **54**, 11169-11186.
3. P. E. Blöchl, *Physical Review B*, 1994, **50**, 17953-17979.
4. J. P. Perdew, K. Burke and M. Ernzerhof, *Phys. Rev. Lett.*, 1996, **77**, 3865-3868.
5. H. J. Monkhorst and J. D. Pack, *Physical Review B*, 1976, **13**, 5188-5192.
6. I. Yeriskin and M. Nolan, *J. Phys.: Condens. Matter*, 2010, **22**, 135004.
7. V. Bellière, G. Joorst, O. Stephan, F. M. F. de Groot and B. M. Weckhuysen, *The Journal of Physical Chemistry B*, 2006, **110**, 9984-9990.
8. M. Guo, J. Lu, Y. Wu, Y. Wang and M. Luo, *Langmuir*, 2011, **27**, 3872-3877.
9. M. V. Ganduglia-Pirovano, J. L. F. Da Silva and J. Sauer, *Phys. Rev. Lett.*, 2009, **102**, 026101.
10. M. Nolan, S. C. Parker and G. W. Watson, *Surf. Sci.*, 2005, **595**, 223-232.
11. M. Nolan, *Chem. Phys. Lett.*, 2010, **499**, 126-130.
12. K. Ahn, D. S. Yoo, D. H. Prasad, H.-W. Lee, Y.-C. Chung and J.-H. Lee, *Chem. Mater.*, 2012, **24**, 4261-4267.